Chapter 2
Investigations into Biomechanics of the Bladder

At each stage entirely new laws, concepts, and generalizations are necessary, requiring inspiration and creativity to just as great a degree as in the previous one.

P. Anderson

2.1 Biomechanics of the Detrusor

A knowledge of the mechanical properties of the tissue of the bladder wall is crucial for the integration of motor functions into a biologically plausible biomechanical model. The combined study of urine flow in the bladder, the urinary sphincter, and the urethra is called urodynamics. The cystometric technique was first reported by Rose (1927) and has been extensively used since then for both clinical and research purposes. Today, urodynamic investigations remain "the gold standard" and the most definitive tests for the evaluation of organ function objectively through a physiological micturition cycle. They comprise a series of tests which imply the real-time monitoring of changes in bladder volume, intravesical p_{ves}, and abdominal p_{abd}, pressures, uroflowmetry, surface electromyography, and video-urodynamics during subsequent phases of artificial bladder filling and emptying (Schmidt et al. 2002; Nitti 2005). All recordings are made via a urethral catheter and a rectal balloon and acquired data are used to calculate the cumulative bladder capacity V, detrusor pressure $p_{\mathrm{det}}(p_{\mathrm{det}} = p_{\mathrm{ves}} - p_{\mathrm{abd}})$, and its contraction strength T, urine outflow rate Q, and urethral opening pressure and resistance. Although the method provides valuable quantitative information about the overall behavior of the bladder one has to realize that these studies are restricted to the assessment of micturition parameters only which are dependent essentially on theoretical concepts—physiological, mathematical, computational—employed in the evaluation of functionality of the organ.

As a part of urodynamic studies detrusor electromyography (EMG) focuses primarily on recording electrical smooth muscle activity in living animals during active bladder emptying using surface electrodes, attached to the bladder wall, or needle electrodes, directly inserted into the detrusor muscle. This method is being utilized for fundamental studies of bladder muscle physiology, testing the integrity of neural circuits, and intrinsic/extrinsic control mechanisms under normal and pathological conditions (Kinder et al. 1997; 1999, 2001; Ballaro et al. 2001). EMG recordings offer higher spatial resolution and better dynamic estimates of bladder function than the assessment of pressure changes only. Thus, spontaneous slow

R. N. Miftahof and H. G. Nam, *Biomechanics of the Human Urinary Bladder*,
DOI: 10.1007/978-3-642-36146-3_2, © Springer-Verlag Berlin Heidelberg 2013

wave and repetitive spiking activities originating from the detrusor itself have been demonstrated convincingly in in situ experiments on rabbit bladders (Kinder et al. 1997, 2001). The multiple electrode technique positioning along the wall has allowed estimation of the maximum conduction velocity of an arbitrary spike, which is ~ 3 cm/s. The time domain and power spectrum analyses of recorded data clearly indicate the correlation of detrusor electromyogenic activity with intravesical pressure rise (Scheepe et al. 1999). Despite significant advancements in animal EMG studies, no electromyographic recordings have been obtained and verified from human detrusor.

Although a large number of urodynamic studies on isolated and intact animal and human bladders have been carried out to measure their electromechanical activity and an enormous number of publications are available in the open literature, these results do not allow reconstruction of active and passive uniaxial and biaxial force-stretch ratio relationships, evaluation of structural changes in the detrusor and surrounding tissues, and assessment of the spatiotemporal dynamics of variations in mechanical properties during the tension bearing process. Therefore, it is not surprising that credible models of the bladder tissue as a mechanical biologically active continuum have not been constructed yet.

Most experiments on the bladder tissue under simple and complex loading protocols have been conducted on animals and only a few studies have been dedicated to the investigation of the human organ *per se* (Alexander 1971, 1976; Kondo et al. 1972; Coolsaet et al. 1975a, b, 1976; van Mastright et al. 1978; van Mastrigt and Nagtegaal 1981; Andersson et al. 1989; Venegas et al. 1991; Wagg and Fry 1999; Finkbeiner 1999; Sacks 2000; Gloeckner et al. 2002; Gloeckner 2003; Korossis et al. 2009; Nagatomi et al. 2008; Parekh et al. 2010; Wognum 2010). Linear strips for uniaxial stretching were usually collected from different regions of the organ. Since the experiments were performed on the segments removed from the host, it was assumed that the muscle fibers were fully relaxed and the mechanical contribution was attributed to mechanochemically inert components of smooth muscle cells along with elastin and collagen fibers. In vitro quasi-static and dynamic tension tests were performed along two structurally defined orthogonal directions of anisotropy—the longitudinal (λ_l) and circumferential (λ_c). Their orientation coincided with the long and circumferential axes of the bladder, respectively. Assuming the homogeneity of the stress and strain fields and the incompressibility of the tissue, the passive force and stretch ratios $(T^p_{c,l} - \lambda_{c,l})$ were calculated. The interpolation of data in the preferred axes of structural anisotropy yield

$$T^p_{(c,l)} = c_1\left[\exp c_2(\lambda_{(c,l)} - 1) - 1\right], \quad \lambda_{(c,l)} > 1, \tag{2.1}$$

where c_1, c_2 are mechanical constants.

Experimental results have demonstrated that the tissue has nonlinear, pseudoelastic properties and is similar to other biological materials. Analysis of the $T^p_{c,l}(\lambda_{c,l})$ curves has shown a characteristic "triphasic" response with a nonlinear transition between the low and high elastic states (Fig. 2.1). The bladder tissue is compliant at low levels of stretching (phase 1) followed by a highly nonlinear

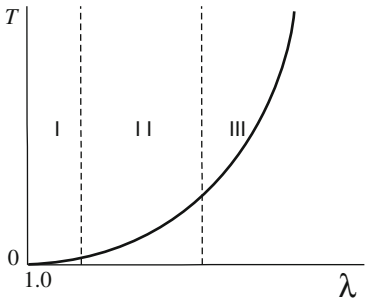

Fig. 2.1 A representative force–stretch ratio curve for a soft biological tissue

transitory phase 2. Specimens demonstrate pure linear elastic behavior for high levels of stretching (phase 3). The representative data for the pig, female rat, and dog urinary bladders are given in Table 2.1.

Overall analysis across different species has revealed that the bladder wall has a considerable inherent inhomogeneity in its material properties, and it does not stretch equally in all directions—it is more compliant circumferentially than longitudinally. It is noteworthy that while insignificant differences between the loading and unloading curves are present due to "biological hysteresis", the force–stretch ratio responses are independent of the stretching rate.

Histoarchitectural correlations with the dynamics of stress–strain development in the bladder wall have revealed that uncoiling of ECM collagen fibers and small randomly oriented crack growth already begins at early stages of filling of the organ. They steadily increase in size as the distension of the bladder proceeds (Fig. 2.2a, b). There is a disrupture in dense packaging of the fibrillary—collagen and elastin—matrix with the expansion and confluence of multiple small fractures. The distribution and orientation of elastin fibers in the bladder wall is region and direction dependent. Most of the elastin is present in the ventral and lateral regions and appear to be oriented predominantly circumferentially. The detrusor muscle and collagen fibers though are most compact within the lower body and trigone regions and are the least affected by distension.

Viscoelastic properties of the bladder wall tissue were studied extensively on uniaxially loaded strips in vitro and whole organ in vivo. The ramp and quasi-static loading protocols were employed in experimental settings. The quasi-linear viscoelastic model was used to describe the strain history dependence and hysteresis (Fung 1993). It assumed that the relaxation function $K(\lambda, t)$ is the product of the pseudoelastic response $T(\lambda)$ and a reduced relaxation function $G(t)$

$$K(\lambda, t) = T_0(\lambda) + \int_0^t T[\lambda(t-\tau)] \frac{\partial G(\tau)}{\partial \tau} \partial \tau \tag{2.2}$$

where

$$G(t) = \frac{1 + c_d[X(t/\tau_2) - X(t/\tau_1)]}{1 + c_d \ln(\tau_2/\tau_1)} \quad \text{for } \tau_1 \le \tau \le \tau_2, \tag{2.3}$$

Table 2.1 The representative data for the pig, female rat, and dog urinary bladders

Species	Phase 1	Phase 2	Phase 3
Pig	$1.0 < \lambda_{c,l} \leq 1.25$	$1.25 < \lambda_{c,l} \leq 1.8$	$\lambda_{\max} \sim 3 \pm 0.2$
	$T^p_{c,l} \sim 0 \div 0.8$ kPa	$T^p_{c,l} \sim 0.8 \div 3.2$ kPa	$T^p_{\max} = 4 \pm 0.5$ kPa
Female rat	$1.0 < \lambda_{c,l} \leq 1.15$	$1.15 < \lambda_{c,l} \leq 1.28$	$\lambda_{\max} \sim 1.3 \pm 0.1$
	$T^p_{c,l} \sim 0 \div 10$ kPa	$T^p_{c,l} \sim 10 \div 65$ kPa	$T^p_{\max} = 100 \pm 25$ kPa
Dog	$1.0 < \lambda_{c,l} \leq 1.05$	$1.05 < \lambda_{c,l} \leq 1.15$	$\lambda_{\max} \sim 1.6 \pm 0.2$
	$T^p_{c,l} \sim 0 \div 38$ kPa	$T^p_{c,l} \sim 38 \div 82$ kPa	$T^p_{\max} = 140 \pm 20$ kPa

and

$$X(t/\tau) = \int_0^\infty (e^{-t}/t)\mathrm{d}t \quad \text{where } (t/\tau) \leq \pi. \tag{2.4}$$

In the above, c_d is the decay parameter, and τ_1, τ_2 are the fast and slow time constants, respectively.

Results of stress relaxation studies have revealed indifference in biomaterial responses to quasi-static, ramp-and-hold and oscillatory modes of loading along the structural axes of anisotropy. There is a shift of the stiffness and damping curves toward smaller frequencies of applied load and a decrease in the slope with higher stress levels indicating that larger stresses result in less relaxation and the damping is more effective at smaller frequencies.

Biaxial tests to investigate in vitro pseudoelastic characteristics of the bladder wall tissue of different animals under quasi-static and dynamic loadings were conducted on square-shaped specimens. These studies allowed the deduction of full in-plane mechanical properties of the tissue. The edges of the specimens were aligned parallel and perpendicular to the orientation of the longitudinal and circular smooth muscle fibers. The experimental protocol to obtain force–stretch ratio curves $T^p_{c,l}(\lambda_c, \lambda_l)$ used constant stretch ratios of λ_1: λ_c.

The in-plane passive $T^p_{c,l}$ forces under biaxial loading are calculated as

$$T^p_{c,l} = \frac{\partial \rho W}{\partial(\lambda_{c,l} - 1)}. \tag{2.5}$$

The most general form of the pseudo-strain energy density function W is

$$\begin{aligned} \rho W = \frac{1}{2}\Big[& c_3(\lambda_1 - 1)^2 + 2c_4(\lambda_1 - 1)(\lambda_c - 1) + c_4(\lambda_c - 1)^2 + \\ & + c_6 \exp\Big(c_7(\lambda_1 - 1)^2 + c_8(\lambda_c - 1)^2 + 2c_9(\lambda_1 - 1)(\lambda_c - 1)\Big)\Big], \end{aligned} \tag{2.6}$$

where ρ is the density of the undeformed tissue.

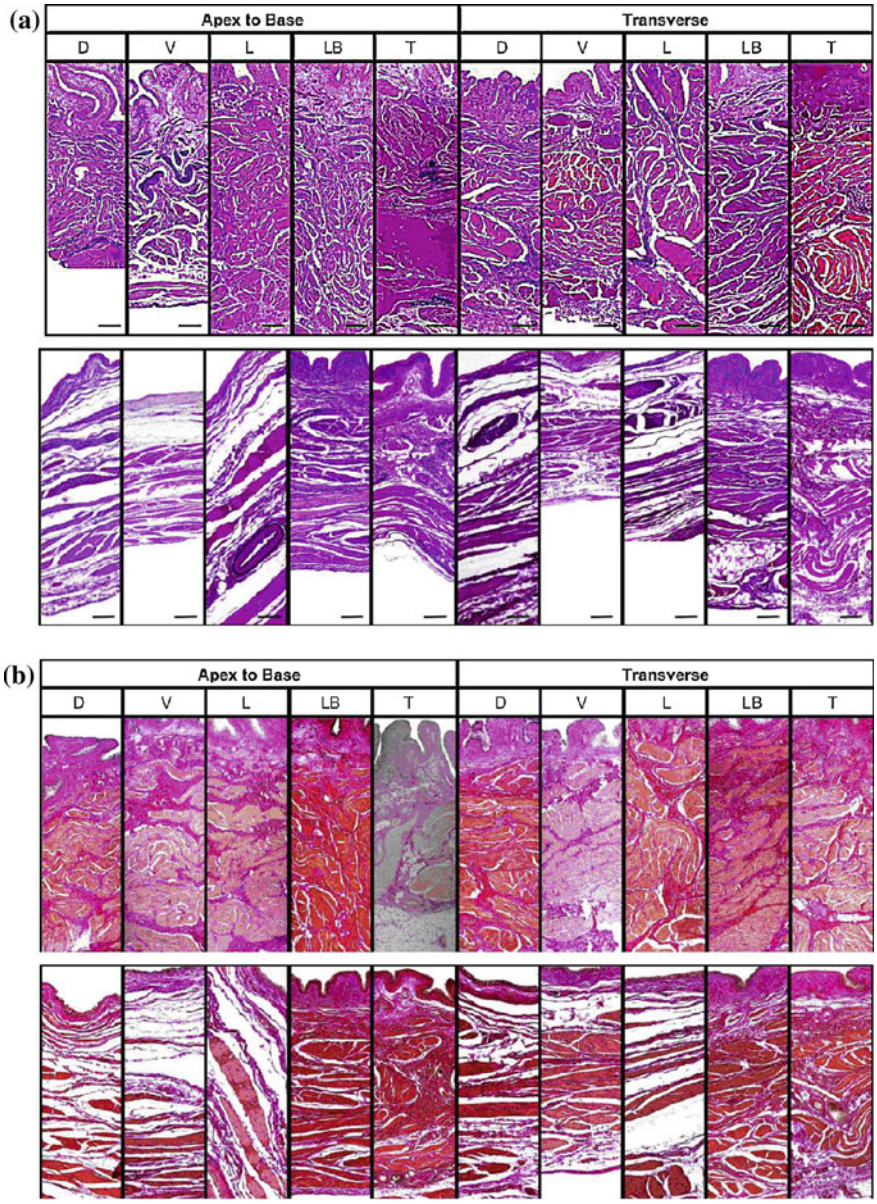

Fig. 2.2 **a** Miller's staining of full thickness samples for elastin from the dorsal (*D*), ventral (*V*), lateral (*L*), lower body (*LB*), and trigone (*T*) regions of nondistended (*upper trace*) and distended porcine bladder, **b** Van Gieson's staining of full thickness samples for collagen and smooth muscle fibers of nondistended and distended porcine bladder. Reproduced with permission from Korossis et al. (Korossis et al. 2009)

Bladders of pigs, rats, and dogs under biaxial loading exhibit a complex response including nonlinear pseudoelasticity, transverse anisotropy, and finite deformability, and no dependence on the stretch rate. The curves $T^{p}_{c,l}(\lambda_c, \lambda_l)$ show that as the stretch ratio in one direction increases gradually, the extensibility along the other decreases (Fig. 2.3). There is a concomitant increase in the stiffness of the biomaterial. The maximum force the tissue can bear during the biaxial tests depends on the ratio $\lambda_l{:}\lambda_c$. Experiments have shown that the shear force applied to the tissue is significantly less $10^{-2}\, T^{p}_{\mathrm{maxc,l}}$ compared with the stretch force. Unfortunately, no experimental results have been obtained from the human urinary bladder for the analysis.

Investigations into uniaxial and biaxial mechanical properties of actively contracting tissue remain the challenge in biomechanics. To the moment this book was written there were no experimental data available on in-plane active behavior of the wall of the urinary bladder. The main problem is to keep specimens physiologically viable and stable, i.e., for in vitro samples to reproduce myoelectrical patterns that are consistent with those observed in vivo. Thus, it is practically impossible to sustain and control simultaneously spiking and contractile activity of smooth muscle syncytia.

Over the years, surprisingly little attention has been given to the problem of constructing constitutive models of the bladder wall. The most common type of mathematical models used for soft tissues are phenomenological, and are usually of a polynomial or exponential form (Palmas and Rigato 1967; Kondo and Susset 1973; Regnier et al. 1983). Thus, earlier proposed descriptions of viscoelastic properties of the tissue employed a combination of Maxwell and Hooke elements. Elastic, time and viscous parameters, and constants of the models were evaluated from experimentally recorded cystometry curves. Despite their robustness and practicality, they do not capture the underlying mechanisms of biomaterial behavior and, therefore, have failed to integrate information about tissue composition and structure with its mechanical properties.

The first detailed research on a multiphase structural constitutive model development for soft tissue with applications to the urinary bladder mechanics has been undertaken by Wognum (2010). Assuming that:

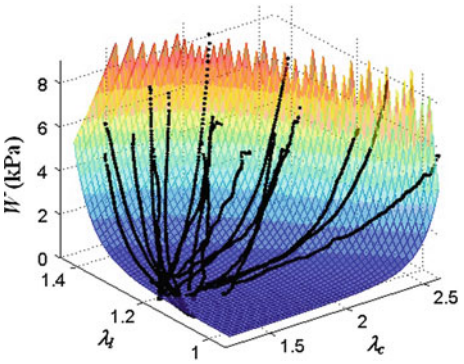

Fig. 2.3 The strain energy function contour and fit of experimental biaxial data (*black lines*) for the rat bladder. Reproduced with permission from Wognum (Wognum 2010)

1. The soft tissue is an idealized network of muscle and undulated (in undeformed state) collagen fibers embedded into a compliant ground matrix;
2. The mechanical net response is the sum of responses of individual fibers; and
3. The tissue is incompressible; and
4. The strain energy density function W satisfies the decomposition.

$$W = \phi_{\mathrm{ECM}} W_{\mathrm{ECM}}(E) + \phi_{\mathrm{SM}} W_{\mathrm{SM}}(E), \tag{2.8}$$

where ϕ_{ECM}, ϕ_{SM} are the extracellular matrix and smooth muscle volume fractions, respectively, and **E** is the Green–Lagrange strain tensor, the Piola–Kirchhoff stress **S** is obtained as

$$S(E) = \frac{\partial W}{\partial E} - l_{\mathrm{m}} C^{-1} = \phi_{\mathrm{ECM}} S_{\mathrm{ECM}}(E_{\mathrm{ECM}}) + \phi_{\mathrm{SM}} S_{\mathrm{SM}}(E_{\mathrm{SM}}) - l_{\mathrm{m}} C^{-1}. \tag{2.9}$$

Here l_{m} is the Lagrange multiplier and **C** is the right Cauchy-Green strain tensor. The subsequent recruitment of fibers during loading in an ensemble of weight bearing elements suggests that a complete stress in the ECM and SM are

$$S_{\mathrm{i}}(E_{\mathrm{i}}) = \eta \phi_{\mathrm{f}} \int_{-\pi/2}^{\pi/2} R(\hat{\theta}) \left\{ \int_{0}^{E_{ens}} D(x) E_{\mathrm{ens}}(\hat{\theta}) dx \right\} \bar{r} \otimes \bar{r} \mathrm{d}\hat{\theta}\, i = \mathrm{ECM},\ \mathrm{SM}, \tag{2.10}$$

where the parameters and functions are referred to the collagen/smooth muscle fiber: η is the modulus, ϕ_{f} is the volumetric fraction, $R(\hat{\theta})$ is the distribution function, $\hat{\theta}$ is the angle orientation in the undeformed configuration, E_{ens} is the fiber ensemble slack strain, $D(x)$ is the recruitment function, $\bar{r}$ is the orientation vector. The exact forms of $R(\hat{\theta})$ and $D(x)$ are assumed to be known a priori. Thus, for collagen fibers the common representation for collagen fibers is bimodal beta distribution, and for smooth muscle—the two-parameter exponential model is widely adopted.

The general nature of the approach has a potential to explain underlying remodeling mechanisms of individual constituents, i.e., the process of uncoiling, straightening, and reorientation of fibers along the direction of the applied force, under normal physiological conditions and to estimate their role in various pathologies.

2.2 Modeling of the Bladder

Publications on mathematical modeling of the biomechanics of the urinary bladder are scarce. The primary focus has been on modeling of the bladder as a reservoir (Regnier et al. 1983; van Beek 1997; Vlastelica et al. 2007; Spirka and Damaser 2007; Korkmaz and Rogg 2007; Fry et al. 2011), its neuronal control mechanisms

(Hosein and Griffiths 1990; Kinder et al. 1999; Bastiaanssen et al. 1996a, b; van Duin et al. 2000; Fernández et al. 2004; Pérez et al. 2008), and the simulation of urine–bladder–urethra interactions during filling and micturition (Damaser and Lehman 1993; Fletcher et al. 1997; Damaser 1999; Křen et al. 2001; Celik et al. 2007; Zang et al. 2010; Kim et al. 2011). All existing models, owing to the number of uncertainties, suffer from considerable biological naiveté that makes them irrelevant in clinical applications. As a result, no comprehensible explanation of normal and pathological lower urinary tract behavior has been proposed so far based on the in silico approach.

The urinary bladder has been typically treated as a thin shell subjected to external and internal quasi-static loads. Initially, it was suggested that the organ could be approximated by a geometrically simple shape—a sphere. Assuming incompressibility, homogeneity, mechanical isotropy, and physical linearity of the wall, Regnier et al. (1983) established the dependence of the inflation pressure on the extension ratios λ_i ($i = 1, 2, 3$)

$$p(\lambda) = \int_1^{\lambda} \frac{1}{\lambda^3 - 1} \frac{\mathrm{d}}{\mathrm{d}\lambda} W(\lambda, \lambda, \lambda^{-2}) \mathrm{d}\lambda, \tag{2.11}$$

where the following form of strain energy function W was

$$W(\lambda, \lambda, \lambda^{-2}) = c(p_0, \dot{p}) + p_0 \mathrm{P}(\dot{p}, \lambda) e^{\alpha(\lambda - 1)}. \tag{2.12}$$

Here $p_0, \dot{p}$ are the initial intravesicular pressure and the rate of pressure change, respectively, $\mathrm{P}(\dot{p}, \lambda)$ is a third degree polynomial, $c(p_0, \dot{p})$ is a constant. The calculated Lagrangian stresses demonstrated a good correlation between the predicted and experimental stress–strain relations recorded from uniaxial loading tests of excised dog bladder strips, as well as slow and rapid cystometry studies performed on the whole organ.

Damaser and Lehman (1993) investigated the role of more complex bladder shapes—the prolate and oblate spheroids—on the intravesicular pressure-volume $p(V)$ response during filling. Results showed that the $p(V)$ curves obtained for prolate and oblate spheroids for a wide range of eccentricity, $0.1 < \varepsilon < 0.9$, did not deviate significantly from the sphere. Later, Damaser (1999) incorporated low muscle tone in the model and reconfirmed their earlier findings.

Křen et al. (2001) studied the interaction of urine with the elastic urethra and bladder during filling and micturition. The bladder-urethra system was modeled as an ellipsoid connected to a cylindrical tube. The wall of the bladder and the urethra, were considered to be isotropic and linear elastic. The urine was a Newtonian fluid and the flow was nonstationary and turbulent. To reproduce dynamic (external body and volume related) forces, "artificial" loading terms were included in the governing system of equations. Although authors provide graphical outputs for the urine velocity outflow, pressure distribution and changes in the configuration of the urinary tract during voiding, the results of simulations are inconclusive, i.e., no detailed quantitative information could be derived from

the data presented about the dynamics of micturition. A similar quasi-empirical analysis of variation in the intravesicular pressure, bladder volume, internal sphincter area, and urine outflow was conducted by Celik et al. (2007). In the model parasympathetic signaling to the detrusor muscle and internal sphincter was achieved through an a priori given signal. It was chosen to be a unit square function for $V_0 < V < V_{\text{crit}}$, where V_{crit} is the critical volume when micturition starts, and a sinusoidal oscillatory function to mimic intermittent voiding. Using experimental curves, e.g., cystograms, and adjusting a number of computational parameters during simulations, the authors achieved satisfactory resemblance quantitatively and qualitatively to clinical observations.

An inverse problem to determine the stress–strain relationships of the bladder wall was considered by Korkmaz and Rogg (2007). Based on the assumption that the organ is a thin spherical shell subjected to complex loading, the wall tension, σ, was calculated from

$$\sigma = \frac{r}{2\delta}(p - p_{\text{abd}}), \tag{2.13}$$

where p_{abd} is the intra-abdominal pressure, r is radius, and δ is the thickness of the sphere. Using actual cystometry and uroflowmetry readings as input data it was possible to reproduce the nonlinear profile of the $\sigma(\lambda)$ curve (λ—stretch ratio) either in the longitudinal or circumferential directions.

van Beek (1997) modeled the bladder as a thick-walled sphere. A special emphasis was given to the evaluation of the effect of muscle fibre orientation and physical nonlinearity of the tissue on the dynamics of deformation of the organ. Three different geometries of fiber winding were studied: the circumferential, longitudinal, and oblique. The total effective Cauchy stress, σ^{e}, was decomposed

$$\sigma^{\text{e}} = \sigma^{\text{e}}_{\text{p}} + \sigma_{\text{a}}, \tag{2.14}$$

where $\sigma^{\text{e}}_{\text{p}}$ is the passive stress is a result of stretch of the connective tissue elements, σ_{a} is the active stress generated by muscle cells. The passive principal stress was obtained as

$$\sigma^{\text{e}}_{\text{p}} = \frac{\partial W(E)}{\partial E}, \tag{2.15}$$

where the strain energy function, W, was chosen in the form

$$W(\text{E}) = b_1 I_{\text{E}}^2 + b_2 II_{\text{E}} + c[\exp(a_1 I_{\text{E}}^2 + a_2 II_{\text{E}}) - 1].$$

Here $I_{\text{E}}, II_{\text{E}}$ are the first and second invariants of E, and a_1, a_2, b_1, b_2, c are empirical constants.

The classical Hill model composed of a parallel passive elastic, $\sigma^{\text{e}}_{\text{p}}$, and a series of passive elastic and contractile elements was used to simulate the active stress. The activation, $A_{\text{r}}(t)$ deactivation, $A_{\text{d}}(t)$, and the length dependence, $A_{\text{l}}(l_{\text{c}})$, functions were introduced to mimic the effect of regulatory mechanisms. They

were derived from experimental curves on single smooth muscle cells of a pig bladder

$$A_r(t) = 1 - \frac{1}{1 + (t/t_r)^4}, \quad A_d(t) = \begin{cases} 1 - \dfrac{1}{1 + [(t_e - t)/t_d]^4}, & t \le t_e \\ 0, & t > t_e \end{cases}, \tag{2.16}$$

$$A_l(l_c) = \frac{(l_c - (l_{max} - l_w))(l_c - (l_{max} + l_w))}{l_w^2}.$$

Here t_r, t_d are the time constants of contraction and relaxation, respectively, l_c is the actual length of a contractile element, and l_{max} is the length of a contractile element at maximal active force, l_w is the rate of curve width.

The cavity pressure during filling was calculated from

$$p = \int_{\lambda_i}^{\lambda_0} \frac{\partial W/\partial \lambda}{\lambda^3 - 1} \, d\lambda, \tag{2.17}$$

where the limits of integration are referred to the stretch ratios of outer and inner radii of the sphere, and during micturition it changed according to urine flow Q,

$$p = i\frac{\partial Q}{\partial t} + RQ, \tag{2.18}$$

here i and R are the inertia and urethral resistance.

Results of numerical simulations in the case of circular winding of muscle fibers demonstrated a gradual change of the spherical configuration of the shell (bladder) to a prolate spheroid during the collection phase and its reversal to the initial state at the end of void. Analysis of stress distribution showed the highest σ^e values at the inner wall in the equator region and the lowest at the poles. The bladder with longitudinal fiber geometry attained the shape of an oblate spheroid at the end of filling with the pattern of stress–strain distribution inverse to the case of circumferential geometry.

While this was a worthy effort by the author, the investigation suffers from the lack of an accurate mathematical formulation of the problem of the dynamics of thick shell. Moreover, the designed numerical algorithm proved to have poor convergence and stability. Therefore, the results *per se* are of a limited scientific value.

A conceptually analogous approach was employed by Vlastelica et al. (2007) in their numerical modeling of the urinary bladder as an axisymmetric thin biologically active shell. The initial configuration of the organ closely resembled the one observed clinically. The wall tissue was assumed to be homogeneous and to possess nonlinear elastic properties. However, the supposition is valid for "passive" biomaterials only and becomes invalid when any muscle activity is present or suspected. Results of simulations of the passive relaxation and detrusor activation phases showed that maximum circumferential stress occurred at the lower

part of the bladder and at the fundus. The body of the organ experienced a uniform axial and circumferential stress distribution throughout.

Although the mathematical models described above have provided useful insights into the investigation of clinical disorders related to bladder hypertony and urethral obstruction, they lack valid anatomical and physiological inputs, i.e., the neural regulatory elements, internal/external bladder and urethral sphincters, urine flow dynamics and neurotransmission mechanisms, among others. The first plausible attempt to address these issues was undertaken by Bastiaanssen et al. (1996a, b) in their myocybernetic model of the lower urinary tract. Authors exercised a system biology approach to simulate the bladder as a multihierarchical system that integrated neural network, biomechanical, and urodynamic components in one quantitative model. The dynamics of neural excitatory and inhibitory stimuli that trigger detrusor and urethral sphincter contraction and relaxation, respectively, are described in terms of normalized activity functions $f_{\mathrm{aD}}, f_{\mathrm{aS}}$

$$\tau \frac{\mathrm{d}f_{\mathrm{aD}}}{\mathrm{d}t} = \omega_{\mathrm{e}}^{\mathrm{D}} - f_{\mathrm{aD}}\left(1 - \omega_{\mathrm{i}}^{\mathrm{D}}\right) \quad f_{\mathrm{aD}} \in [0, 1] \tag{2.19}$$

$$\tau \frac{\mathrm{d}f_{\mathrm{aS}}}{\mathrm{d}t} = \omega_s - f_{\mathrm{aS}} \quad f_{\mathrm{aS}} \in [0, 1], \tag{2.20}$$

where τ is a time constant, $\omega_e^{\mathrm{D}}, \omega_i^{\mathrm{D}}, \omega_s$ are the excitatory (subscript *e*), inhibitory (*i*), and excitatory somatic (*s*) inputs $\left((\omega_{\mathrm{e}}^{\mathrm{D}}, \omega_{\mathrm{i}}^{\mathrm{D}}, \omega_{\mathrm{s}}) \in [0, 1]\right)$.

Assuming quasi-static isometric contractions the detrusor was treated as a homogeneous incompressible viscoelastic continuum. The total actual tensile stresses in the smooth muscle and sphincter was decomposed into a sum of the active and passive stresses

$$\sigma_{\mathrm{D}} = k_{\mathrm{area}}(f_{\mathrm{aD}}\sigma_{\max}\sigma_{\mathrm{v}}(v_{\mathrm{D}})\sigma_{\mathrm{l}}(l_{\mathrm{D}}) + \sigma_{\mathrm{e}}(l_{\mathrm{D}}) + \sigma_{\mathrm{ve}}(v_{\mathrm{D}})), \tag{2.21}$$

$$\sigma_{\mathrm{S}} = k_{\mathrm{thick}}(f_{\mathrm{aS}}\sigma_{\max}\sigma_{\mathrm{v}}(v_{\mathrm{S}})\sigma_{\mathrm{l}}(l_{\mathrm{S}}) + \sigma_{\mathrm{e}}(l_{\mathrm{S}})). \tag{2.22}$$

Here, all functions are normalized on [0,1], $\sigma_{\max}$, $\sigma_{\mathrm{l}}(l_{\mathrm{D}})$, $\sigma_{\mathrm{l}}(l_{\mathrm{S}})$ are the maximal and actual isometric stresses of the detrusor and urethral sphincter, respectively, $\sigma_{\mathrm{v}}(v_{\mathrm{D}})$, $\sigma_{\mathrm{v}}(v_{\mathrm{S}})$ are velocity-dependent stresses obtained at optimal length of muscle fibers that satisfy the Hill equation, $\sigma_{\mathrm{e}}(l_{\mathrm{D}}), \sigma_{\mathrm{e}}(l_{\mathrm{S}}), \sigma_{\mathrm{ve}}(v_{\mathrm{D}})$ are the elastic and viscoelastic stresses, k_{area}, k_{thick} are the ratio of the cross-sectional area of the detrusor taken at optimal muscle fiber length to the actual area and thickness of the sphincter, respectively.

The bladder was considered to be a thin spherical isotropic shell and the sphincter was a cylinder. The intravesicular and active sphincter pressures were calculated as: $p_{\mathrm{D(S)}} = \sigma_{\mathrm{D(S)}} \ln(r^{\mathrm{o}}_{\mathrm{D(S)}}/r^{i}_{\mathrm{D(S)}})$, where $r^{o}_{\mathrm{D(S)}}, r^{i}_{\mathrm{D(S)}}$ are the outer and internal radii of the shell and the sphincter, respectively. With regard to the passive elastic properties of the urethral sphincter, an exponential relationship between the radius of the urethra and urine pressure was selected.

Steady flow assumption was made to describe flow in different parts of the bladder-urethra system. The flow Q was obtained from

$$Q = \sqrt{\frac{p_{\mathrm{u}}}{R_{\mathrm{t}}(R_i, A_i)}} \quad i = u_{\mathrm{p}}, u_{\mathrm{d}} \tag{2.23}$$

where p_{u} $(p_{\mathrm{u}} = p_{\mathrm{S}})$ is the liquid pressure in the urethra, and $R_{\mathrm{t}}(R_i, A_i)$ is the total resistance of the distal urethra, a function of the resistance and cross-sectional areas of the proximal and distal parts of the urethra.

In the above model, most parameters have both physiological and physical meanings. Therefore, it was possible for authors to define a range of their variation and measure their actual values. Despite its mathematical and biological naiveté, the model results clearly resembled traces obtained from urodynamic studies. Several other models of the lower urinary tract have been proposed which are, to a certain extent, variations of the Bastiaanssen et al. model. However, all of these models lack solid biological and mechanical foundations by design. Therefore, they cannot answer important questions related to pathophysiological changes that occur in signal transduction mechanisms and biomechanical activity, or predict the effects of pharmacological interventions in various diseases.

Finally, a new class of models have emerged recently, to study the dynamics of urinary flow in the bladder and urethra. They are a result of advancements in computational, software and imaging technology, MRI with digital three-dimensional image processing, and image reconstruction, in particular. The approach focuses primarily on detailed description of geometry and the application of solid and fluid mechanic principles to simulate the lower urinary tract anatomical structures and their functions. Although existing models are still biologically and biomechanically deficient, i.e., no active forces and deformations are generated in the bladder and the urethra during micturition, and no regulatory (parasympathetic and sympathetic) inputs are present, they offer original insight into the dynamics of bladder-urethra-urine flow. For example, the occurrence of a secondary flow at the base of the bladder, which is a result of the action of convective acceleration of fluid and viscous friction, has been demonstrated using a computational model by Zang et al. (2010). Computational models, when they reach the desired level of biological consistency, reliability, and robustness in their design and performance, will undeniably become an indispensable clinical tool. They will help solve puzzling intricacies of pathophysiological mechanisms of diseases, which are inaccessible to investigations in vivo, and will facilitate the development of rational pharmacotherapies that do not have deleterious side effects.

We shall employ a combined reduction—integration systems biology approach as the main conceptual strategy to study the urinary bladder. The approach is being proven as the most effective and successful scientific method for an in-depth investigation of individual biological components and to understand the nonlinear multiparametric dynamic interrelationships among them. We shall start our analysis with the essentials that are required to understand the concepts involved in development of a model of the urinary bladder. Any reader familiar with the

subject can proceed directly to Chap. 6. Then we shall study the biomechanics of the detrusor fasciculus, followed by the detrusor—intramural ganglion arrangement, and, finally, shall provide a holistic perspective of the urinary bladder as a thin biologically active self-controlled system.

References

Alexander RS (1971) Mechanical properties of the urinary bladder. Am J Physiol 220:1413–1421
Alexander RS (1976) Series elasticity of urinary bladder smooth muscle. Am J Physiol 231:1337–1342
Andersson KE, Kronström A, Bjerle P (1989) Viscoelastic properties of the normal human bladder. Scand J Urol Nephrol 23:115–120
Ballaro A, Mundy AR, Fry CH, Craggs MD (2001) A new approach to recording the electromyographic activity of detrusor smooth muscle. J Urol 166(5):1957–1961
Bastiaanssen EHC, van Leeuwen JL, Vanderschoot J, Redert PA (1996a) A myocybernetic model of the lower urinary tract. J Theor Biol 178:113–133
Bastiaanssen EHC, Vanderschoot J, van Leeuwen JL (1996b) State–space analysis of a myocybernetic model of the lower urinary tract. J Theor Biol 180:215–227
Celik IB, Varol A, Bayrak C, Nanduri JR (2007) A one dimensional mathematical model for urodynamics. In: Proceedings of FEDSM2007, 5th ASME/JSME fluids engineering conference, July 30–Aug 2, 2007, San Diego, p 1–7
Coolsaet BLRA, van Duyl WA, van Mastrigt R, Schouten JW (1975a) Viscoelastic properties of bladder wall strips. Invest Urol 12:351–355
Coolsaet BLRA, van Duyl WA, van Mastrigt R, van der Zwart A (1975b) Visco-elastic properties of the bladder wall. Urol Int 30:16–26
Coolsaet BLRA, van Mastrigt R, van Duyl WA, Huygen RE (1976) Viscoelastic properties of bladder wall strips at constant elongation. Invest Urol 13(6):435–440
Damaser MS (1999) Whole bladder mechanics during filling. Scand J Urol Nephrol Suppl 201:51–58
Damaser MS, Lehman SL (1993) Does it matter, the shape of the bladder? Neurourol Urodynam 12:227–280
Fernández DR, Chamizo JMG, Pérez FM, Payá AS (2004) Modeling the distributed control of the lower urinary tract using a multiagent system. In: Modeling decisions for artificial intelligence, Lecture Notes on Computer Science, vol 3131. Springer, New York, pp 1–5
Finkbeiner AE (1999) In vitro responses of detrusor smooth muscle to stretch and relaxation. Scand J Urol Nephrol Suppl 201:5–11
Fletcher W, Smith FT, Fry C (1997) A computer simulation of micturition. Private report
Fry CH, Sadananda P, Wood DN, Thiruchelvam N, Jabr RI, Clayton R (2011) Modeling the urinary tract—computational, physical, and biological methods. Neurourol Urodynam 309:692–699
Fung YC (1993) Biomechanics: mechanical properties of living tissues, 2nd edn. Springer, New York 568 p
Gloeckner DC (2003) Tisssue biomechanics of the urinary bladder wall. Thesis, Doctor Phil, University Pittsburgh, USA
Gloeckner DC, Sacks MS, Fraser MO, Somogyi GT, de Groat WC, Chancellor MB (2002) Passive biaxial mechanical properties of the rat bladder wall after spinal cord injury. J Urol 167:247–252
Hosein RA, Griffiths DJ (1990) Computer simulation of the neural control of bladder and urethra. Neurourol Urodynam 9:601–618

Kim J, Lee MK, Choi B (2011) A study of the fluid mechanical urinary bladder simulator and reproduction on human urodynamics. Int J Precis Eng Manufact 12(4):679–685
Kinder MV, Gommer ED, Janknegt RA,van Waalwijk van Doorn ESC (1997) A method for the electromyographic mapping of the detrusor smooth muscle. Arch Physiol Biochem 105(7):673–690
Kinder MV, Bastiaanssen EHC, Janknegt RA, Marani E (1999) The neuronal control of the lower urinary tract: a model of architecture and control mechanisms. Arch Physiol Biochem 107:203–222
Kinder MV, Bos R, Janknegt R, Marani E (2001) Demonstration of spontaneous and stretch induced urinary bladder EMG in the living rabbit. Arch Physiol Biochem 109(5):389–403
Kondo A, Susset JG (1973) Physical properties of the urinary bladder detrusor muscle. A Mechanical model based upon the analysis of stress relaxation curve. J Biomech 6:141–151
Kondo A, Susset JG, Lefaivre J (1972) Viscoelastic properties of bladder I. Mechanical model and its mathematical analysis. Invest Urol 10(2):154–163
Korkmaz I, Rogg B (2007) A simple fluid-mechanical model for prediction of the stress-strain relation of the male urinary bladder. J Biomech 40:663–668
Korossis S, Bolland F, Southgate J, Ingham E, Fisher J (2009) Regional biomechanical and histological characterization of the passive porcine urinary bladder: implications fro augmentation and tissue engineering strategies. Biomaterials 30:266–275
Křen J, Horák M, Zát'ura F, Rosenberg M (2001) Mathematical model of the male urinary tract. Biomed Pap 145(2):91–96
Nagatomi J, Toosi KK, Chancellor MB, Sacks MS (2008) Contribution of the extracellular matrix to the viscoelastic behaviour of the urinary bladder wall. Biomech Model Mechanobiol. doi:10.10007/s10237-007-0095-9
Nitti VW (2005) Pressure flow urodynamic studies: the gold standard for diagnosing bladder outlet obstruction. Rev Urol 7:S14–S21
Palmas G, Rigato M (1967) Confronto fra il compotamento viscoelastico della vescica urinaria e quello di un modello meccanico ideale. Atti Acad Fisiocrit Siena Med Fis 16(2):1731–1763
Parekh A, Cigan AD, Wognum S, Heise RL, Chancellor MB (2010) Ex vivo deformations of the urinary bladder during whole bladder filling: contributions of extracellular matrix and smooth muscle. J Biomech 43:1708–1716
Pérez FM, Chamizo JMG, Payá AS, Fernández DR (2008) A robust model of the neuronal regulator of the lower urinary tract based on artificial neural networks. Neurocomputing 71:743–754
Regnier C, Kolsky H, Richardson PD, Ghoinem GM, Susset JG (1983) The elastic behavior of the urinary bladder for large deformations. J Biomech 16(11):915–922
Rose DK (1927) Cystometric bladder pressure determinations: their clinical importance. J Urol 17:487–501
Sacks MS (2000) Biaxial mechanical evaluation of planar biological materials. J Elastic 61:199–246
Scheepe JR, Bross S, Schumacher S, Braun P, Weiss J, Alken P, Jünemann KP (1999) Recording the evoked canine detrusor electromyogram. Neurourol Urodyn 18(6):687–695
Schmidt F, Shin P, Jorgensen TM, Djurhuus JC, Constantinou CE (2002) Urodynamics patterns of normal male micturition: influence of water consumption on urine production and detrusor function. J Urol 168:1458–1463
Spirka TA, Damaser MS (2007) Modelling of physiology of the urinary tract. J Endourol 21:294–299
Van Beek AJ (1997) A finite element model of the urinary bladder. Private report, ISBN 90-5282-738-9
Van Duin F, Rosier PFWM, Benelmans BLH, Wijkstra H, Debruyne FMJ, van Oosterom A (2000) Comparison of different computer models of the neural control system of the lower urinary tract. Neurourol Neurodynam 12:289–310
van Mastright, Coolsaet BLRA, van Duyl WA (1978) Passive properties of the urinary bladder in the collection phase. Med Biol Eng Comput 16:471–482

van Mastrigt R, Nagtegaal JC (1981) Dependence of the viscoelastic response of the urinary bladder wall on strain rate. Med Biol Eng Comput 19(3):291–296
Venegas JG, Woll JP, Woolfson SB, Cravalho EG, Resnick N, Yalla SV (1991) Viscoelastic properties of the contracting detrusor II: experimental approach. Am J Physiol 261:364–375
Vlastelica I, Veljkovic D, Stojanovic B, Rosic M, Kojic M (2007) Modeling urinary bladder deformation within passive and active regimes. J Serb Soc Comput Mech 1:129–134
Wagg A, Fry CH (1999) Viscoelastic properties of isolated detrusor smooth muscle. Scand J Urol Nephrol Suppl 201:12–18
Wognum S (2010) A multi-phase structural constitutive model for insights into soft tissue remodelling mechanisms. Doctoral Thesis, University of Pittsburgh, USA, p 255
Zang XJ, Li XY, Wang JL (2010) Computational fluid dynamics model of bladder-urethra system for SUI. In: IFMBE proceedings of 6th World Congress Biomechanics, vol 31. pp 1495–1498

http://www.springer.com/978-3-642-36145-6

Biomechanics of the Human Urinary Bladder

Miftahof, R.N.; Nam, H.G.

2013, XXI, 177 p. 43 illus., 10 illus. in color., Hardcover
ISBN: 978-3-642-36145-6